Automatic detection and classification of radiolucent lesions in the mandible on panoramic radiographs using a deep learning object detection technique

Yoshiko Ariji, DDS, PhD,[a] Yudai Yanashita, BE,[b] Syota Kutsuna, BE,[b] Chisako Muramatsu, PhD,[c] Motoki Fukuda, DDS,[d] Yoshitaka Kise, DDS, PhD,[d] Michihito Nozawa, DDS,[d] Chiaki Kuwada, DDS,[e] Hiroshi Fujita, PhD,[f] Akitoshi Katsumata, DDS, PhD,[g] and Eiichiro Ariji, DDS, PhD[h]

Objective. The aim of this study was to investigate whether a deep learning object detection technique can automatically detect and classify radiolucent lesions in the mandible on panoramic radiographs.

Study Design. Panoramic radiographs of patients with mandibular radiolucent lesions of 10 mm or greater, including ameloblastomas, odontogenic keratocysts, dentigerous cysts, radicular cysts, and simple bone cysts, were included. Lesion labels, including region of interest coordinates, were created in text format. In total, 210 training images and labels were imported into the deep learning GPU training system (DIGITS). A learning model was created using the deep neural network DetectNet. Two testing data sets (testing 1 and 2) were applied to the learning model. Similarities and differences between the prediction and ground-truth images were evaluated using Intersection over Union (IoU). Sensitivity and false-positive rate per image were calculated using an IoU threshold of 0.6. The detection performance for each disease was assessed using multiclass learning.

Results. Sensitivity was 0.88 for both testing 1 and 2. The false-positive rate per image was 0.00 for testing 1 and 0.04 for testing 2. The best combination of detection and classification sensitivity occurred with dentigerous cysts.

Conclusions. Radiolucent lesions of the mandible can be detected with high sensitivity using deep learning. (Oral Surg Oral Med Oral Pathol Oral Radiol 2019;128:424−430)

Patients who visit dental clinics often undergo panoramic radiography, and the resulting radiographs often show incidental lesions in areas other than that with the patient's main complaint.[1,2] Techniques for computer-aided diagnosis of lesions on panoramic radiographs have advanced, and they now include such tasks as the prediction of osteoporosis,[3,4] and the diagnosis of bisphosphonate-related osteonecrosis[5] and maxillary sinusitis.[6]

Recently, deep convolutional neural networks (CNNs) have been developed and applied in many medical imaging fields, where they have accomplished various tasks, including image classification,[7-9] object detection,[10-15] and semantic segmentation.[16-18] Within our research group, we have achieved high accuracy in the diagnosis of maxillary sinusitis[19] and extra roots in mandibular first molars,[20] by using a deep CNN applied to panoramic radiographs.

However, although the methods for object detection in medical imaging fields have been rapidly progressing, object detection on panoramic radiographs can still be challenging.[10-15] One such method, the DetectNet, is a deep CNN for object detection using the NVIDIA DIGITS deep learning training system. It performs feature extraction and prediction of object classes with the use of bounding boxes per grid square.[15,21-23]

The purpose of this study was to evaluate the performance of a deep learning object detection technique for the automatic detection and classification of mandibular radiolucent lesions on panoramic radiographs. Targeting only a single lesion cannot provide the amount of data required for the deep learning procedures. Therefore, 5 radiolucent lesions (ameloblastomas, odontogenic keratocysts, dentigerous cysts, radicular cysts, and simple bone cysts) that occur

Statement of Clinical Relevance

Radiolucent lesions of the mandible could be automatically detected on panoramic radiography with high performance using deep learning. The results of this study will be useful for diagnostic support in panoramic radiography.

[a]Associate Professor, Department of Oral and Maxillofacial Radiology, Aichi-Gakuin University School of Dentistry, Nagoya, Japan.
[b]Postgraduate student, Department of Electrical, Electronic and Computer Faculty of Engineering, Gifu University, Gifu, Japan.
[c]Associate Professor, Department of Electrical, Electronic and Computer Faculty of Engineering, Gifu University, Gifu, Japan; Currently, Faculty of Data Science, Shiga University, Shiga, Japan.
[d]Associate Professor, Department of Oral and Maxillofacial Radiology, Aichi-Gakuin University School of Dentistry, Nagoya, Japan.
[e]Part-Time lecturer, Department of Oral and Maxillofacial Radiology, Aichi-Gakuin University School of Dentistry, Nagoya, Japan.
[f]Professor, Department of Electrical, Electronic and Computer Faculty of Engineering, Gifu University, Gifu, Japan.
[g]Professor, Department of Oral Radiology, Asahi University School of Dentistry, Mizuho, Japan.
[h]Professor, Department of Oral and Maxillofacial Radiology, Aichi-Gakuin University School of Dentistry, Nagoya, Japan.
Received for publication Mar 7, 2019; returned for revision May 11, 2019; accepted for publication May 25, 2019.

2212-4403/$-see front matter
https://doi.org/10.1016/j.oooo.2019.05.014

relatively frequently in the mandible were targeted in this investigation.

MATERIALS AND METHODS

This study was approved by the ethics committee of our university (No. 496) and was performed in accordance with the tenets of the Declaration of Helsinki.

Patients

Patients were selected from the imaging database of our institution and had been imaged between 2005 and 2018. The digital panoramic radiographs of all patients were obtained using a Veraview Epocs system (J. Morita Mfg Corp., Kyoto, Japan). The standard parameters included a tube voltage of 75 kV, tube current of 9 mA, and acquisition time of 16 seconds.

The inclusion criteria were presence of a radiolucent lesion in the mandible and histopathologic verification of the diagnosis. All lesions were at least 10 mm in diameter. Panoramic radiographs of 210 patients were identified for use in the training data set. The sites of lesions were the molar region (molar or molar and ramus) in 142 cases (67.6%); the premolar region (premolar, premolar and molar, or premolar and molar and ramus) in 34 cases (16.2%); and the anterior region (anterior, anterior and premolar, or anterior and premolar and molar) in 34 cases (16.2%). The histopathologic diagnoses included 31 ameloblastomas, 33 odontogenic keratocysts, 66 dentigerous cysts, 68 radicular cysts, and 12 simple bone cysts (Table I). The study included 128 men and 82 women (age range 15−85 years; median age 45 years).

For validation purposes, 2 data sets were prepared. The "Testing 1" data set was used for the purpose of evaluating the performance of the learning model with abundant data. It included panoramic radiographs of 50 of the patients in the training data set. The histopathologic diagnoses included 7 ameloblastomas, 8 odontogenic keratocysts, 16 dentigerous cysts, 16 radicular cysts, and 3 simple bone cysts (see Table I). This data set included 32 men and 18 women (age range 18−87 years; median age 49 years). The "Testing 2" data set was used for the purpose of evaluating performance with completely new data and consisted of panoramic radiographs from 25 different patients. This newly collected data set included 3 ameloblastomas, 6 odontogenic keratocysts, 8 dentigerous cysts, 7 radicular cysts, and 1 simple bone cyst (see Table I). This data set included 18 men and 7 women (age range 19−84 years; median age 49 years).

Table I. Numbers of training and testing data sets

	Training data set	*Testing 1 data set*	*Testing 2 data set*
Ameloblastomas	31	7	3
Odontogenic keratocysts	33	8	6
Dentigerous cysts	66	16	8
Radicular cysts	68	16	7
Simple bone cysts	12	3	1
Total	**210**	**50**	**25**

Preparation of the imaging data sets

The digital panoramic radiographs were downloaded in the bitmap format (.BMP) from the image database of our hospital. A pretrained "DetectNet" for panoramic radiographs was set to an image resolution of 900 × 900 pixels. Therefore, all images were cropped to a size of 900 × 900 pixels for use in the training and testing data sets.

Annotation procedure

A single radiologist set the regions of interest (ROIs) by using arbitrarily sized rectangles to include each lesion and recorded the upper left (x1, y1) and lower right (x2, y2) coordinates of the ROIs with the use of ImageJ software (National Institutes of Health, Bethesda, MD) (Figure 1). The ROIs ranged from 64 to 450 pixels (median 112 pixels) in width, and 70 to 360 pixels (median 122 pixels) in height. The label for each lesion, which included these coordinates, was created in text form for each item of the imaging data.

Deep learning procedure

The deep learning system was implemented on an NVIDIA GeForce GTX 11 GB-GPU workstation (NVIDIA

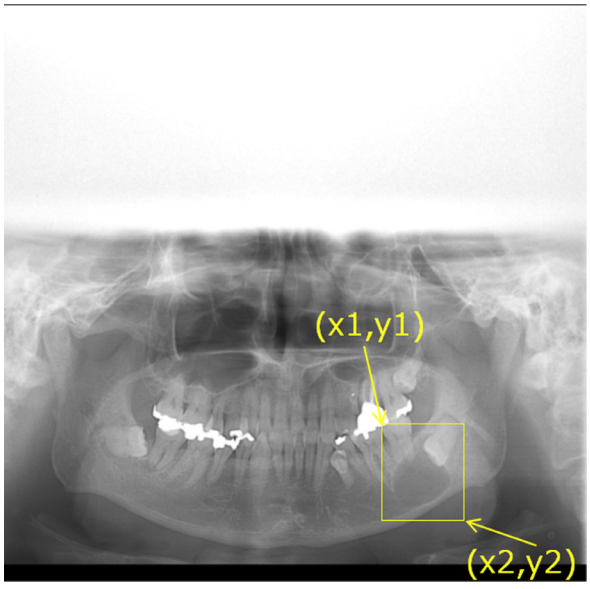

Fig. 1. Method for measuring the coordinates for creating labels. An arbitrarily sized rectangular region of interest (ROI) is set on a digital panoramic radiograph of 900 × 900 pixels. The upper left (x1, y1) and lower right (x2, y2) coordinates of the ROI are recorded.

Corp., Santa Clara, CA) with 128 GB of memory. The training procedures for object detection were performed with use of the deep CNN DetectNet architecture (Figure 2) implemented with the NVIDIA DIGITS (https://developer.nvidia.com/digits) version 5.0 library on the Caffe framework. DetectNet is a neural network created independently by NVIDIA; it has 5 main parts: (1) data ingest and augmentation; (2) a fully convolutional network (FCN); (3) loss function measurement; (4) bounding box clustering; and (5) mean average precision calculation.[15] DIGITS was used to train the network. We used the adaptive moment estimation (Adam) solver, with 0.0001 as the base learning rate.

The training images and labels data sets, as well as the testing (validation) images and labels data sets, were imported into the DIGITS library. The training processes were conducted for 500 epochs, and a learning model was obtained. The number of epochs was determined in such a manner that accuracy of the model became high and stable and the error in prediction using training data approached zero.

Testing procedure

Two kinds of testing image data sets were applied to the learning model, and the predictions of radiolucent lesions of the mandible were obtained. When the presence of radiolucent lesions was predicted, the red-colored bounding boxes were superimposed over the panoramic radiographs.

Evaluation methods

The similarities and differences between predicted images and ground-truth images were evaluated using Intersection over Union (IoU) for each patient. IoU is the most popular evaluation metric used in the object detection benchmarks.

$$\mathrm{IoU} = \mathrm{S}(\mathrm{P} \cap \mathrm{G})/\mathrm{S}(\mathrm{P} \cup \mathrm{G}),$$

where S is the area, P is the predicted bounding box in which the learning model predicted the presence of a lesion, and G is the ground-truth bounding box that actually had a lesion. IoU is, therefore, the ratio of the area where the 2 boxes overlap (S[P∩G]) to the total combined area of the 2 boxes (S[P∪G]). The larger the value of IoU, the more accurate will be the prediction. In this study, the IoU threshold for determining whether the lesions could be detected was set at 0.6.[11] That is, when the IoU was 0.6 or more, it meant that lesion detection was correctly predicted.

For the evaluation of prediction performance of lesion detection, the sensitivity and false-positive rate per image were calculated. *Sensitivity* was defined as the proportion of regions correctly predicted by the model among those that actually existed. *False-positive rate per image* was defined as the proportion of incorrect detections occurring per image.

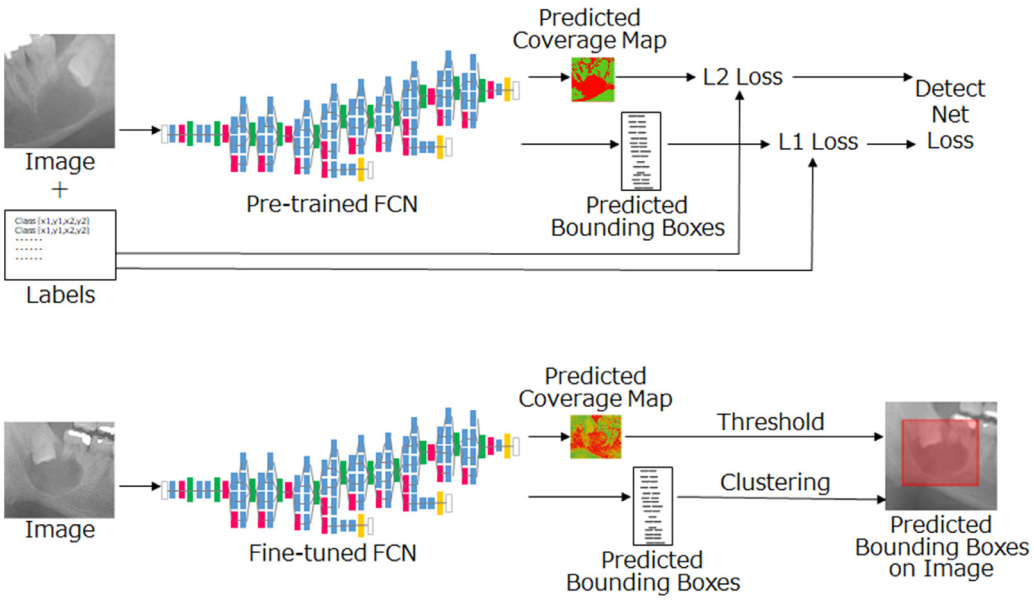

Fig. 2. Workflow of DetectNet. Training processes *(top row)*: Data layers ingest 3 training images and labels, and transformer layers perform inline data augmentation. A pre-trained fully convolutional network (FCN) performs feature extraction and prediction of object classes and bounding boxes per grid square. Loss functions simultaneously measure the error in the 2 tasks of predicting the object coverage (L2 loss) and object bounding box corners per grid square (L1 loss). Testing processes *(bottom row)*: A clustering function produces the final set of predicted bounding boxes during the testing processes. The predicted bounding box is the area in which the learning model predicts the presence of a lesion. When the presence of a radiolucent lesion is predicted, the red-colored bounding boxes are superimposed over the panoramic radiographs. The threshold value was set at 0.6.

Comparison of the detection and classification for each lesion

Multiclass learning was performed by using the learning model obtained earlier as a pretrained model. Ameloblastomas were defined as class 1, odontogenic keratocysts as class 2, dentigerous cysts as class 3, and radicular cysts as class 4.

The number of simple bone cysts was small; therefore, they were excluded for multiclass learning of detection and classification. The training procedure was performed for 500 epochs, and the detection and classification performance were determined using training data set 1. For classification of lesions, the predicted bounding boxes of class 1 (ameloblastomas) were displayed in red, those of class 2 (odontogenic keratocysts) in light blue, those of class 3 (dentigerous cysts) in green, and those of class 4 (radicular cysts) in purple.

RESULTS

Time taken for the deep learning procedure

The time taken to import the training and validation image and label data sets into the DIGITS library was 13 seconds. It took 3 hours for the 500 epoch training processes to achieve a learning model. Each testing procedure took 13 seconds.

Detection performance

The results using the 50-image testing 1 data set and the 25-image testing 2 data set are shown in Table II. The sensitivity for detection of the mandibular radiolucent lesions was 0.88 with both data sets. A sensitivity of 0.88 indicated that the learning model could correctly predict the presence of lesions in 88% of the actual lesions. The false-positive rate per image was 0.00 for the testing 1 data set, and 0.04 for testing 2 data set. A false-positive rate per image of 0.04 indicated that the learning model incorrectly predicted the presence of lesions at nonlesional areas in 1 of 25 images from the testing 2 data set.

Examples of the results of radiolucent lesion detection

Examples of the successful detection of lesions are shown in Figure 3. Large lesions were well detected when their borders were well-defined (see Figure 3A).

Table II. Performance in the detection of radiolucent lesions using testing 1 and testing 2 data sets

	Detection	
	Sensitivity	*False-positive rate per image*
Testing 1 data set	0.88	0.00
Testing 2 data set	0.88	0.04

A dentigerous cyst was well detected not only by its well-defined border but also by its positional information, as shown in Figure 3B.

In the failed example shown in Figure 4, a small lesion with a poorly-defined border and faint radiolucency was not detected.

Comparison of detection and classification for each lesion

The results of the multiclass object detection are shown in Table III. The term *detection sensitivity* refers to the rate at which the learning model correctly detected the lesion as a result of multiclass learning. The term *classification sensitivity* refers to the rate at which the learning model correctly classified the lesion. The detection sensitivity and classification sensitivity were 0.71 and 0.60, respectively, for ameloblastomas, 1.00 and 0.13 for odontogenic keratocysts, 0.88 and 0.82 for dentigerous cysts, and 0.81 and 0.77 for radicular cysts. All odontogenic keratocysts were detected, but the classification sensitivity was very low (Figure 5). Ultimately, the best detection and classification performance was achieved for dentigerous cysts.

DISCUSSION

Deep learning technologies can be applied to the interpretation of medical images in a number of ways, including classification,[7-9] object detection,[10-15] and semantic segmentation.[16-18]

However, few studies have described the application of deep learning to the interpretation of panoramic radiographs frequently exposed in dental clinics. De Tobel et al. evaluated deep learning for determining the developmental stage of mandibular third molars on panoramic radiographs,[24] and our previous study demonstrated the diagnosis of maxillary sinusitis on panoramic radiographs using deep learning, with a high accuracy of 87.5%.[19] We also examined whether extra roots of mandibular first molars can be diagnosed using deep learning applied to panoramic radiographs and reported a high accuracy of 87.4%.[20] There are also reports evaluating deep learning for the classification of osteoporosis.[25,26]

The main advantage of panoramic radiography is that it allows for the detection of a variety of lesions, such as those of teeth, jaws, temporomandibular joints, maxillary sinuses, and salivary stones.[1,2] For busy and/or inexperienced dentists, automatic detection of lesions is considered clinically more useful than image classification because it can contribute to reducing oversight of lesions other than the patient's main complaint. However, there are few reports on deep learning for lesion detection on panoramic radiographs.

The most important part of a deep learning system is the convolutional neural network (CNN). There are

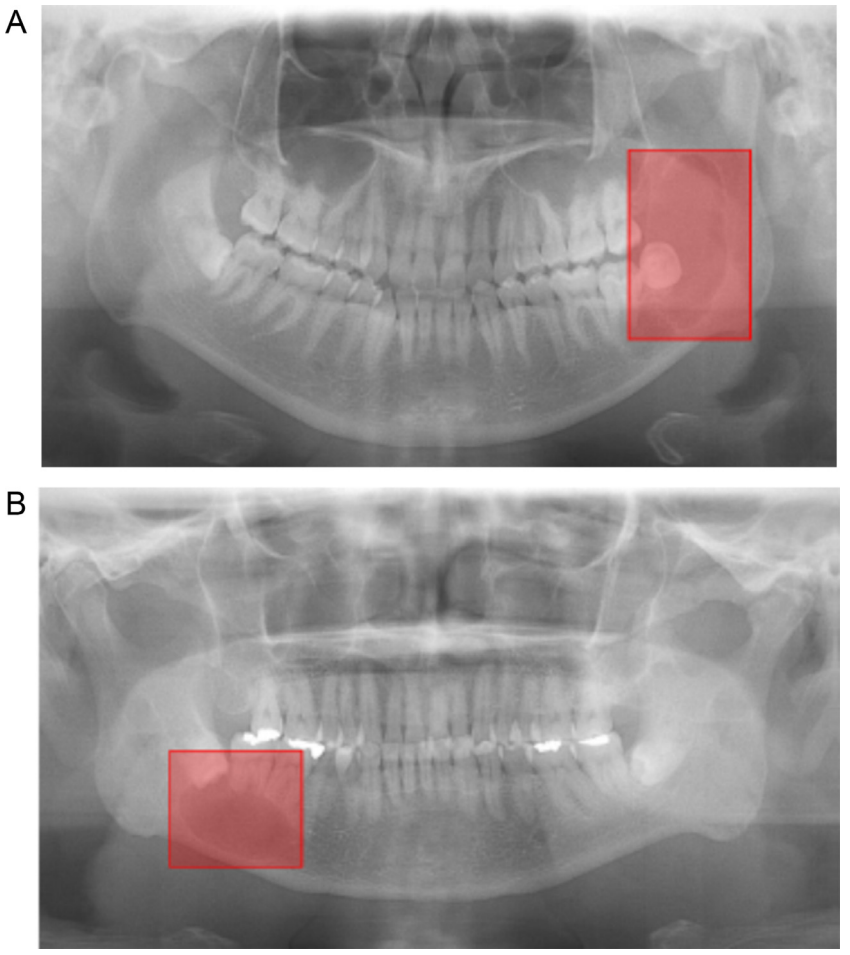

Fig. 3. Examples of successful lesion detections. **A,** A 36-year-old man with an ameloblastoma. This large lesion was well detected by a well-defined border. **B,** A 61-year-old man with a dentigerous cyst. This lesion was well detected by a combination of a well-defined border and position information.

many open source CNN object detection architectures, including region-based CNN (R-CNN), You Only Look Once (YOLO), and DetectNet.[10-15,21]

The most frequently investigated CNN is Faster R-CNN, which is a derivative of R-CNN.[10-13] In Faster R-CNN, feature maps are first extracted from the input

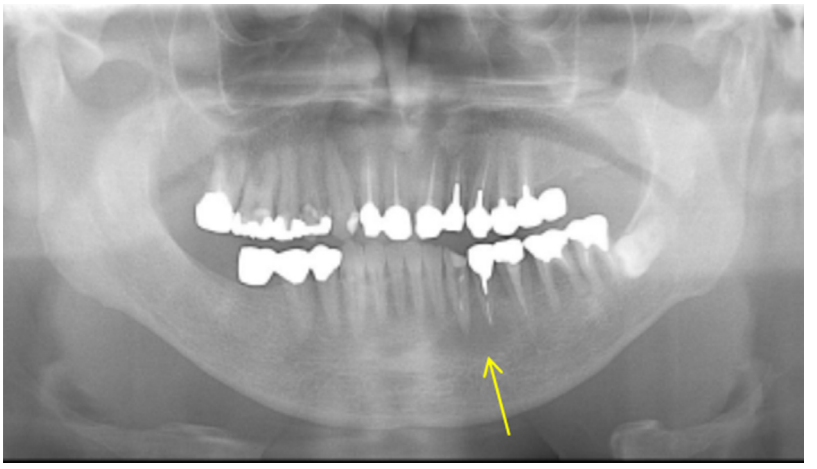

Fig. 4. Example of a failed lesion detection. A 56-year-old man with a radicular cyst. The lesion was situated in the left mandibular canine and first premolar region *(arrow)*, but this small lesion with poorly-borders and faint radiolucency could not be detected.

Table III. Performance in the detection and classification of each type of lesion using testing I data set

	Detection sensitivity	*Classification sensitivity*
Ameloblastomas	0.71	0.60
Odontogenic keratocysts	1.00	0.13
Dentigerous cysts	0.88	0.82
Radicular cysts	0.81	0.77

image. These maps are then passed through a region proposal network, which returns object proposals. Finally, these maps are classified, and the bounding boxes are predicted.[10-13] Faster R-CNN yields better detection accuracies compared with other networks but has higher computational time costs.[13]

Al-Masni et al. reported using YOLO,[14] which divides the image into grids and performs object recognition for each grid. Compared with R-CNN, YOLO has a somewhat low accuracy for object detection, but has a fast processing speed.[14]

DetectNet is a neural network created independently by NVIDIA. It has 5 main parts: (1) data ingest and augmentation; (2) FCN; (3) loss function measurement; (4) bounding box clustering; and (5) mean average precision calculation.[15,21-23] Yu et al.[21] were able to detect broadleaf weeds with a high performance rate of 99% with the use of DetectNet, with a reported image processing speed of 42 ms. Suleymanova et al.[15] reported a high positive correlation between manual quantification and the use of DetectNet in counting the numbers of astrocytes in the brains of rats.

The full CNN of DetectNet is basically the same as that of GoogLeNet, differing only in that the input, last pooling, and output layers are removed.[15] To significantly speed up the training process, the pretrained GoogLeNet is usually applied.[15] Because the CNN contains millions of parameters, training is insufficient with low numbers of annotated images.[13] Therefore, the pretrained CNN usually offers optimal performance for object detection.[11]

This study demonstrated high detection performance, with sensitivity of nearly 90% for radiolucent lesions. Dentigerous cysts, with both high detection and classification sensitivities, were the best-detected lesions probably because of their preferred sites; these cysts are most frequently found in the mandibular third molars. In the cases of failed detection, lesions could not be detected because of their small size, poorly-defined borders, and/or faintly radiolucent image. Small lesions provide less information for discrimination of their classes, and therefore, more training data will be needed to successfully detect such lesions.[13] In the regions with few texture features, lesions may still not be dentified.[11] The number of individual lesion samples was small in the multiclass studies in the present investigation, so further study will be needed to draw a conclusion.

There are some limitations to this study. Deep learning requires a large amount of labeled training data.[11] If more training data were to be provided, the models have the potential to become significantly more accurate.[10]

External testing data would be necessary to judge the generalizability of the CNN.[13] We did not use external data in this study. The use of the same images in the training and testing 1 data sets may have improved the sensitivity results. Therefore, the testing 2 data set contained completely different lesions. The fact that sensitivity and false-positive rates were virtually identical for both testing data sets confirmed the beneficial effects of the CNN.

For training object detection-based CNNs, a process of manually annotating individual lesions is necessary.[21] There are few publicly available pixel-level annotated

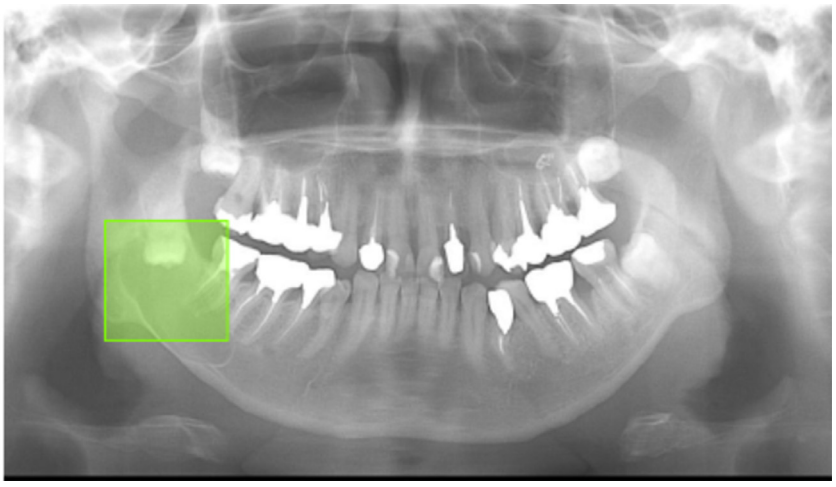

Fig. 5. Example of a successful lesion detection but failed classification after multiclass learning. A 53-year-old man with an odontogenic keratocyst. A lesion in the right third molar region was detected but misclassified as a dentigerous cyst.

data sets,[10] and this manual process is time consuming and labor intensive.[21] Last, we only used annotations from one expert radiologist, and, therefore, we could not evaluate interobserver variability.[13]

In the future, semantic segmentation will be necessary, and if fully automated segmentation is shown to be fast, reproducible, and user-friendly, it will be applied in clinical practice.[18] This study was limited to mandibular radiolucent lesions, so further studies to consider maxillary lesions are needed.

CONCLUSIONS

Our study confirmed that a deep learning system using DIGITS and DetectNet had high values of detection and classification sensitivity in the detection of radiolucent lesions of the mandible. In the future, we will establish a faster and more accurate system that uses a large amount of labeled external training data.

ACKNOWLEDGMENT

We thank Karl Embleton, PhD, from Edanz Group (www.edanzediting.com/ac) for editing a draft of this manuscript.

REFERENCES

1. Ribeiro A, Keat R, Khalid S, et al. Prevalence of calcifications in soft tissues visible on a dental pantomogram: a retrospective analysis. *J Stomatol Oral Maxillofac Surg*. 2018;119:369-374.
2. Resnick CM, Dentino KM, Garza R, Padwa BL. A management strategy for idiopathic bone cavities of the jaws. *J Oral Maxillofac Surg*. 2016;74:1153-1158.
3. Muramatsu C, Horiba K, Hayashi T, et al. Quantitative assessment of mandibular cortical erosion on dental panoramic radiographs for screening osteoporosis. *Int J Comput Assist Radiol Surg*. 2016;11:2021-2032.
4. Nakamoto T, Taguchi A, Ohtsuka M, et al. A computer-aided diagnosis system to screen for osteoporosis using dental panoramic radiographs. *Dentomaxillofac Radiol*. 2008;37:274-281.
5. Demiralp KÖ, Kurşun-Çakmak ES, Bayrak S, Akbulut N, Atakan C, Orhan K. Trabecular structure designation using fractal analysis technique on panoramic radiographs of patients with bisphosphonate intake: a preliminary study. *Oral Radiol*. 2019;35:23-28.
6. Ohashi Y, Ariji Y, Katsumata A, et al. Utilization of computer-aided detection system in diagnosing unilateral maxillary sinusitis on panoramic radiographs. *Dentomaxillofac Radiol*. 2016;45:20150419.
7. Perek S, Kiryati N, Zimmerman-Moreno G, Sklair-Levy M, Konen E, Mayer A. Classification of contrast-enhanced spectral mammography (CESM) images. *Int J Comput Assist Radiol Surg*. 2019;14:249-257.
8. Yasaka K, Akai H, Abe O, Kiryu S. Deep learning with convolutional neural network for differentiation of liver masses at dynamic contrast enhanced CT: a preliminary study. *Radiology*. 2018;286:887-896.
9. Wang X, Yang W, Weinreb J, et al. Searching for prostate cancer by fully automated magnetic resonance imaging classification: deep learning versus non-deep learning. *Sci Rep*. 2017;7:15415.
10. Ribli D, Horváth A, Unger Z, Pollner P, Csabai I. Detecting and classifying lesions in mammograms with deep learning. *Sci Rep*. 2018;8:4165.
11. Li H, Weng J, Shi Y, et al. An improved deep learning approach for detection of thyroid papillary cancer in ultrasound images. *Sci Rep*. 2018;8:6600.
12. Onieva JO, Serrano GG, Young TP, Washko GR, Carbayo MJL, Estépar RSJ. Multiorgan structures detection using deep convolutional neural networks. *Proc SPIE Int Soc Opt Eng*. 2018: 10574. pii: 1057428.
13. Koitka S, Demircioglu A, Kim MS, Friedrich CM, Nensa F. Ossification area localization in pediatric hand radiographs using deep neural networks for object detection. *PLoS One*. 2018;13:e0207496.
14. Al-Masni MA, Al-Antari MA, Park JM, et al. Simultaneous detection and classification of breast masses in digital mammograms via a deep learning YOLO-based CAD system. *Comput Methods Programs Biomed*. 2018;157:85-94.
15. Suleymanova I, Balassa T, Tripathi S, et al. A deep convolutional neural network approach for astrocyte detection. *Sci Rep*. 2018;8:12878.
16. Fu M, Wu W, Hong X, et al. Hierarchical combinatorial deep learning architecture for pancreas segmentation of medical computed tomography cancer images. *BMC Syst Biol*. 2018;12:56.
17. Jackson P, Hardcastle N, Dawe N, Kron T, Hofman MS, Hicks RJ. Deep learning renal segmentation for fully automated radiation dose estimation in unsealed source therapy. *Front Oncol*. 2018;8:215.
18. Blanc-Durand P, Van Der Gucht A, Schaefer N, Itti E, Prior JO. Automatic lesion detection and segmentation of 18 F-FET PET in gliomas: a full 3 D U-Net convolutional neural network study. *PLoS One*. 2018;13:e0195798.
19. Murata M, Ariji Y, Ohashi Y, et al. Deep-learning classification using convolutional neural network for evaluation of maxillary sinusitis on panoramic radiography [e-pub ahead of print]. *Oral Radiol*. doi:10.1007/s11282-018-0363-7, accessed Dec 11, 2018
20. Hiraiwa T, Ariji Y, Fukuda M, et al. A deep-learning artificial intelligence system for assessment of root morphology of the mandibular first molar on panoramic radiography. *Dentomaxillofac Radiol*. 2018;47:20180218.
21. Yu J, Sharpe SM, Schumann AW, Boyd N.S. Detection of broadleaf weeds growing in turfgrass with convolutional neural networks [e-pub ahead of print]. *Pest Manag Sci*. doi:10.1002/ps.5349, accessed Jan 22, 2019.
22. Rajpura PS, Bojinov H, Hegde RS. Object detection using deep CNNs trained on synthetic images. Ithaca, NY: Cornell University; 2017. Available at: https://arxiv.org/abs/1706.06782.
23. Tao A, Barker J, Sarathy S. Detect Net: deep neural network for object detection in DIGITS. 2016. Available at: https://devblogs.nvidia.com/parallelforall/detectnet-deep-neural-network-object-detection-digits/.
24. De Tobel J, Radesh P, Vandermeulen D, Thevissen PW. An automated technique to stage lower third molar development on panoramic radiographs for age estimation: a pilot study. *J Forensic Odontostomatol*. 2017;2:42-54.
25. Chu P, Bo C, Liang X, et al. Using octuplet Siamese network for osteoporosis analysis on dental panoramic radiographs. *Conf Proc IEEE Eng Med Biol Soc*. 2018;2018:2579-2582.
26. Lee JS, Adhikari S, Liu L, Jeong HG, Kim H, Yoon S.J. Osteoporosis detection in panoramic radiographs using a deep convolutional neural network-based computer-assisted diagnosis system: a preliminary study [e-pub ahead of print]. *Dentomaxillofac Radiol*. doi:10.1259/dmfr.20170344, accessed Jul 13, 2018.

Reprint requests:

Yoshiko Ariji,
Department of Oral and Maxillofacial Radiology
Aichi-Gakuin University School of Dentistry
2-11 Suemori-dori
Chikusa-ku
Nagoya 464-8651
Japan.
yoshiko@dpc.agu.ac.jp